Geomechanics and Engineering, *Vol. 33, No. 3 (2023) 301-315*
https://doi.org/10.12989/gae.2023.33.3.301

Effect of cohesion of infill materials on the performance of geocell-reinforced cohesive soil subgrade

Yang Zhao[1], Zheng Lu[*1,2], Jie Liu[**3], Lei Ye[4], Weizhang Xu[4] and Hailin Yao[1]

[1]*State Key Laboratory of Geomechanics and Geotechnical Engineering, Institute of Rock and Soil Mechanics, Chinese Academy of Sciences, Wuhan 430071, China*
[2]*Hubei Key Laboratory of Geo-Environmental Engineering, Wuhan 430071, China*
[3]*Xinjiang Transportation Planning Survey and Design Institute Co., Ltd., Urumqi 830006, China*
[4]*Anhui He chuang New Synthetic Materials Co., Ltd., Huainan 232221, China*

(*Received December 12, 2022, Revised March 8, 2023, Accepted March 10, 2023*)

Abstract. Adopting cohesive soil as geocell-pocket infill materials is not fully accepted by researchers in the field of road engineering. The cohesion that may inhibit the lateral limitation of geocells is a common vital idea that exists within every researcher. However, the influence of infill materials' cohesion on geocell-reinforced performance is still not thoroughly determined. The mechanism behind this still needs to be studied in depth. This study initially discussed the relationship between subgrade bearing capacity, geocells' contribution to reinforced performance, and infill materials' cohesion (IMC). A law was proposed that adopting the soil with high cohesion as infill materials benefited the subgrade bearing capacity, but this was attributed to the superior mechanical properties of infill materials rather than geocells' contribution. Moreover, the vertical and lateral deformation of subgrade, coupling shear stress and confining stress of geocells, and deformation of geocells were deeply studied to analyze the mechanism that high cohesion can inhibit the geocells' contribution. The results indicate that the infill materials with high cohesion result in the total displacement of the subgrade toward to deeper depth, not the lateral direction. These responses decrease the vertical coupling shear stress, confining stress, and normal displacement of geocell walls, which weaken the lateral limitation of geocells.

Keywords: bearing capacity; cohesive soil subgrade; FLAC3D; geocells; numerical modeling

1. Introduction

Road subgrade and pavement structure are subject to deterioration over time due to traffic loads and long-term climatic factors, which can lead to pavement cracking and reduced service life. Especially during the fill period, with the booming infrastructure development worldwide, many road constructions faced the embarrassing situation of using poorly performing soils for their construction. Hence, a very critical problem waiting for addressing is how to decrease the thickness of the base layer during the fill period or to take effective methods to enhance the strength and bearing capacity of the weak subgrade (Kumar *et al.* 2019).

Recently, geosynthetics reinforcing the base layer (Sheikh and Shah 2020, Khalaj *et al.* 2015) and subgrade structures (Luo *et al.* 2021, Latha 2011) have been widely accepted by many researchers. As a sort of special geosynthetics, the honeycombed-shaped geocells have a three-dimensional lateral limitation system to improve the apparent cohesion of the soil and benefit the bearing capacity of road structures. The researchers and users can use soils to fill the opening geocell pockets to make the geocell-reinforced layer perform similarly to the semi-rigid plates to disperse vertical stress (Biswas and Mittal 2017, Song and Tian 2019, Altay *et al.* 2021, Ardakani and Namaei 2021).

In the past, various laboratory model tests (Suku *et al.* 2016, George *et al.* 2021, Hegde and Sitharam 2016, Tafreshi *et al.* 2018), field tests (Luo *et al.* 2021), and numerical studies (Saride *et al.* 2013) were carried out by several investigators have highlighted the potential benefits of using geocell in the base layer and subgrade reinforcement. The dynamic and cyclic loading model tests proved that using geocell reinforcement in the base layer could improve the resilient modulus and decrease the cumulative plastic deformation (George *et al.* 2021, Thakur *et al.* 2017, Suku *et al.* 2016, Thakur *et al.* 2012). Using the smaller thickness base layer with geocell reinforcement can achieve the same performance as a thicker base layer. Plus, our research group members, Luo *et al.* (2021), also conducted a series of field tests to study the contribution of geocells to subgrade or roadbed structure, with the evaluation parameters: average penetration, resilient modulus, and dynamic stress. The experimental and numerical results suggested that geocells can enhance the strength of roadbeds to decrease the subgrade deflection and weak the dynamic stress on subgrade structure. Moreover, many researchers adopted the static model tests and numerical simulations because this method could avoid the defects that dynamic waves bounced at the boundary for

*Corresponding author, Professor
E-mail: zlu@whrsm.ac.cn
**Corresponding author, Senior Engineer
E-mail: hfutliujie@163.com

ISSN: 2005-307X (Print), 2092-6219 (Online)

dynamic model tests and that many uncontrollable factors exited in the field tests. Dehkordi *et al.* (2019), Kargar and Mir Mohammad Hosseini (2018), Pokharel *et al.* (2010) all studied the improvement of bearing capacity with geocell reinforcement base layer, in terms of pressure-settlement response. In general, the high geocell walls, the high geocell modulus, multiple layers of geocell, and the rough surface of walls can increase the bearing capacity of road structures. On the other hand, the deeper buried depth of the geocell and the large opening pocket diameter are not beneficial to improving the bearing capacity. Moghaddas Tafreshi *et al.* (2016), Dutta and Mandal (2016), Moghaddas Tafreshi *et al.* (2021), Biswas *et al.* (2013) all reported the similar conclusions.

It is worth noting that the beneficial effect of geocells in the reinforcement of base and subgrade is found to be substantial when cohesionless soil (sandy or granular materials) is used as infill materials. Several researchers used them to fill the opening geocell pockets (Sitharam and Hegde 2013, Sireesh *et al.* 2009, Tafreshi and Dawson 2010). Two reasons are causing that: the first one is that aggregates, sand or other cohesionless soil are the common materials for the base layer; the second reason is that geocell can bring more enhanced performance due to lacking cohesion (Pokharel *et al.* 2010). It is very suitable for reinforcing the base layer and sand subgrade structures due to adopting the soil that is identical to the subgrade, as infill materials can save many transportation costs. The construction personnel can not be necessary to transport the sand soil to fill geocell pockets specially. However, for the cohesive soil subgrade reinforcement, e.g., the reinforced engineerings shown in the paper of our research group (Luo *et al.* 2021), the feasibility of using the cohesive subgrade soil as infill materials needs to be determined. Also, there are many reclaimed asphalt pavement bases (Thakur *et al.* 2012, George *et al.* 2021) and quarry waste bases (Pokharel *et al.* 2010), in which the infill materials' cohesion (IMC) inevitably exists. Hence, this idea involves two critical questions: Can the cohesive soil be used as infill materials? What does the influence of cohesive soil as infill materials on geocell-reinforced performance?

There are some interesting studies, in which adopting cohesive soil as infill materials is to improve the bearing capacity. (Sitharam and Sireesh 2005, Chaney *et al.* 2000, Thallak *et al.* 2007). Few but significant researches have been carried out in this area to compare the reinforced performance of cohesive and non-cohesive soil. Pokharel *et al.* (2010) demonstrated that limited improvement was observed for the geocell-reinforced quarry waste base layer. As we know, geocells can increase the apparent cohesion of non-cohesive soil (Bathurst and Karpurapu 1993) because of the lateral limitation. The cohesion of quarry waste itself probably weak the reinforced performance. It was a pity that there was no mechanism to explain this reason in their paper. However, Hegde and Sitharam (2015) reported the total opposite conclusions. There is no significant difference in the reinforced performance with cohesive and non-cohesive soil as infill materials. Biswas *et al.* (2021) also obtained a similar result as Hegde and Sitharam (2015). Different researchers could obtain the exact opposite conclusions, which makes us necessary to determine the suitability of using cohesive soil as infill materials and the applications of geocells in road structures.

This study further advances our research group's previous studies (Luo *et al.* 2021, Lu *et al.* 2019, Xian 2019). In the previous cohesive subgrade reinforced engineering, the authors found that, for the reinforcement of cohesive soil subgrade, it is time-consuming and laborious if sandy soils need to be transported to fill geocell pockets. However, the existing studies are insufficient to determine whether adopting the subgrade soil as infill materials can obtain excellent reinforced performance. Hence, this study focuses on evaluating the influence of IMC on geocell-reinforced performance based on the numerical simulations of the static plate load test. By changing the IMC, the pressure-settlement responses of subgrade were initially analyzed, and then the contributions of geocells were evaluated by the bearing capacity improvement factor (I_f) and the percentage of geocells contribution (PGC_N). Authors attempted to seek the relationship between geocells contribution, subgrade bearing capacity, and IMC. Further, to explain this relationship in the mechanism, the vertical and lateral deformation of subgrade, coupling shear stress and confining stress of geocells, and deformation of geocells were deeply analyzed and discussed based on the geocell-reinforced cases with different infill materials.

2. Validation of a numerical model

Verification of the correctness of the calculation is essential for numerical simulation studies. In this study, the plate load test of geocell reinforced base layer conducted by Gedela and Karpurapu (2021a), Gedela and Karpurapu (2021b) were cited to validate the numerical results by using FLAC^{3D}. The numerical model size was kept the same as plate load tests in the FLAC^{3D} program for the unreinforced and geocell-reinforced cases. It was worth noting that for the unreinforced case, the model dimension was 1.8 m × 1.8 m × 0.65 m. However, the height of the geocell-reinforced model was 0.67 m (see Fig. 1). In the test, the soft subgrade (0.5 m) and the base layer (0.15 m) made up the unreinforced case, while there was another sand cover (0.02 m) on the surface of base layer for the geocell-reinforced case. Detailed descriptions of the model test can be obtained from the paper of Gedela and Karpurapu (2021b). The bottom boundary was fixed at three displacement directions for all numerical models. Plus, four lateral boundaries were also fixed in the normal direction. By doing this, the rigid tank could be omitted to reduce the computational effort.

The Mohr-Coulomb constitutive model was adopted to be close to the soil behavior. Oliaei and Kouzegaran (2017) also used this model in numerical studies. In addition, geocells were modeled by the geogrid elements, which were assigned the CST plane-stress element that only resisted the tensile load (Itasca 2018). In terms of the geocell-soil interface, the Mohr-Coulomb yield criterion was set in FLAC^{3D}. Detailed calculated parameters are presented in Table 1.

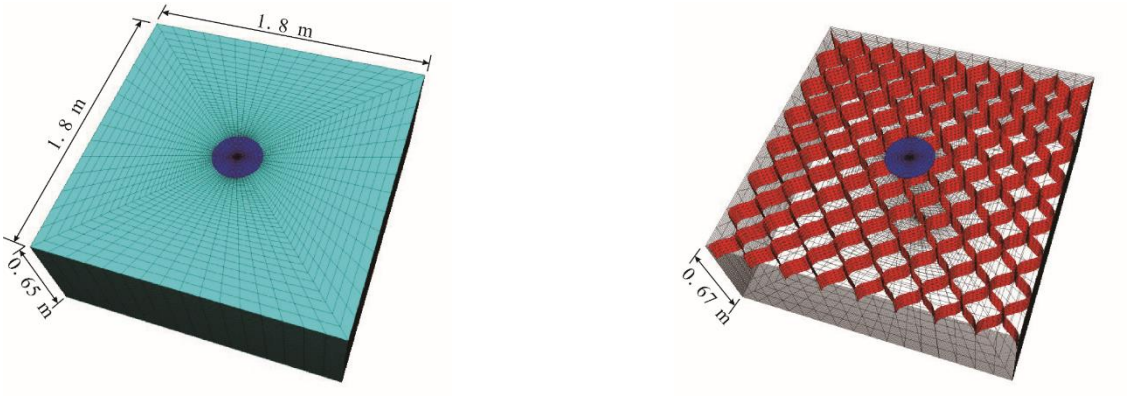

(a) (b)

Fig. 1 The model of (a) unreinforced and (b) geocell-reinforced sections generated in FLAC^{3D}

Table 1 Properties of geocell and different infill materials in numerical modeling (Gedela and Karpurapu 2021b)

Material and model parameters	Value
EPS	
Bulk modulus, K (MPa)	1.71
Shear modulus, G (MPa)	1.8
Poisson's ratio, υ	0.11
Cohesion, c (kPa)	37.5
Friction, φ (°)	2
Density, ρ (kg/m^3)	19.6
Sand	
Young modulus, E (MPa)	35
Poisson's ratio, υ	0.35
Cohesion, c (kPa)	0
Friction, φ (°)	44
Dilation, ψ (°)	11
Density, ρ (kg/m^3)	1721
HDPE geocells	
Weld distance (mm)	356
Cell depth (mm)	150
Strip thickness (mm)	1.5
Young modulus, E (MPa)	235
Poisson's ratio, υ	0.45
Interface shear modulus k_i (MPa/m)	4.4
Interface cohesion, c_i (kPa)	0
Interface friction, φ_i (°)	41

In numerical calculations, the normal stress or gridpoint force can not be applied directly to the loading area because this method represents the purely flexible footing. Instead, the vertical displacement in the loading area (300 mm diameter) was added at a constant velocity to simulate the rigid plate. The lateral velocity (displacement) was fixed to simulate the rough bottom of the loading plate. A series of FISH codes were developed during the analysis to calculate the loading pressure. The unbalanced force of each gridpoint in the loading area was added together, and then the value of applied pressure was obtained by the total unbalanced force divided by the loading area.

In Fig. 2, it can be seen that the numerical results are in good agreement with the experimental results. The provision of geocell locating in base layer improves the

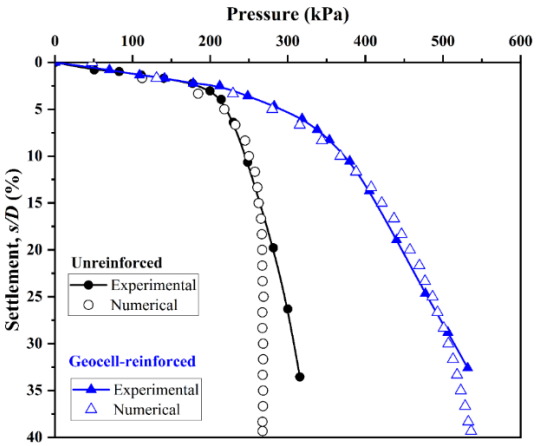

Fig. 2 Validation of numerical studies

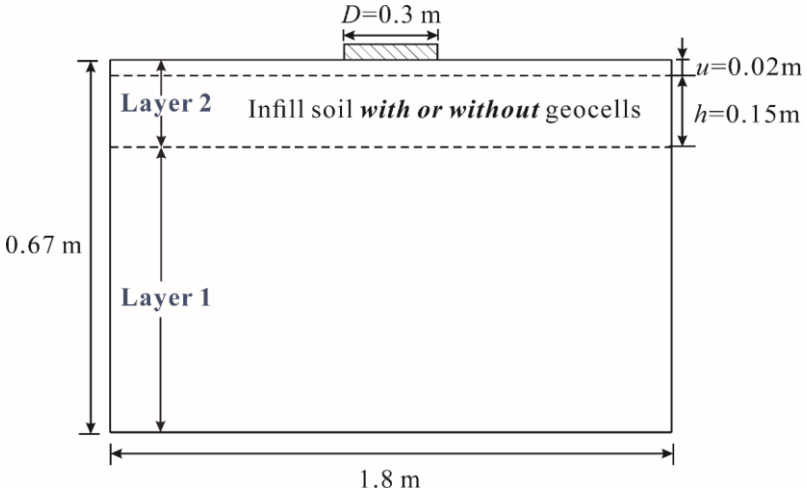

Fig. 3 Scheme diagram of numerical models

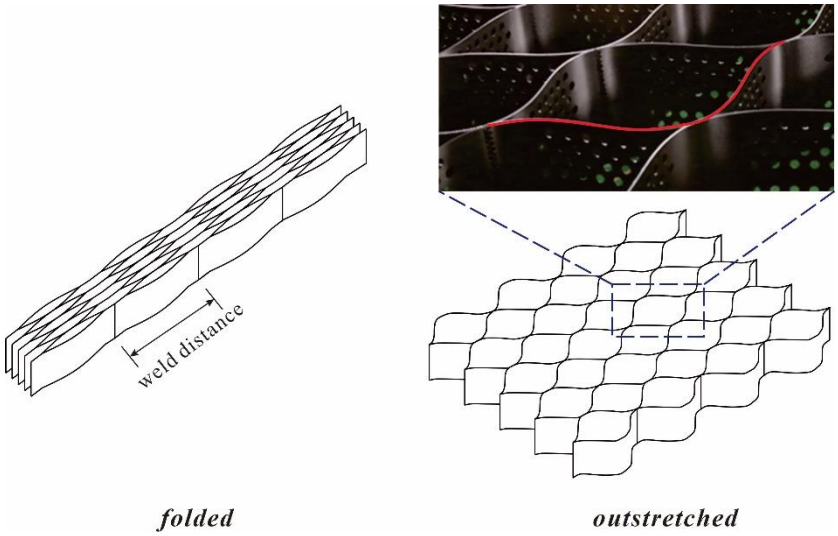

Fig. 4 Introduction of weld distance of geocells

bearing capacity of road structure. Pressure–settlement response of unreinforced and geocell-reinforced cases presents punching shear and general shear type failure, respectively. The geocell-reinforced layer can disperse pressure over a wider area and mobilize more soil to resist applied load due to geocells' semi-rigid nature and lateral limitation.

3. Numerical models of geocell-reinforced soft subgrade

This study extended the validated numerical model to the geocell-reinforced cohesive soil subgrade with the subgrade soil as infill materials. Ari and Misir (2021) also used a similar approach to extend the validated model for numerical calculations. Fig. 3 shows the schematic diagram of numerical models. In Fig. 3, it can be noted that the subgrade is divided into Layer 1 and Layer 2. The numerical model dimensions, constitutive models, boundary conditions, and increment of the footing vertical displacement all kept the same as those of the validated model. However, the mechanical parameters of Layer 1 were determined from the cohesive soil after one freeze-thaw cycle to simulate the soft cohesive soil. Detailed experimental plans and conclusions can be found in Lu *et al.* (2019) and Xian (2019) papers. The influence of IMC on the reinforced performance was studied by changing the cohesion of Layer 2. The unreinforced cases with different cohesion of Layer 2 were all calculated for comparison and determining the actual contribution of geocells. In this study, the height of unreinforced and geocell-reinforced numerical models was all kept at 0.67 m.

HDPE honeycomb-shaped geocells with 356 mm and 660 mm weld distance, and 150 mm height were chosen for calculations. Fig. 4 presents the schematic form of weld distance (red line in this figure) to be more descriptive and understandable. The opening pocket area was larger than the circle plate for the weld distance of 660 mm. On the other hand, walls were within the loading area for the geocell with the weld distance of 356 mm. By doing this, the influence of IMC on geocell-soil interaction under

Table 2 Parameters used in numerical models

Material and model parameters	Value
Cohesive soil (Layer 1)	
Young modulus, E (MPa)	4.0
Poisson's ratio, υ	0.3
Cohesion, c (kPa)	20
Friction, φ (°)	20
Density, ρ (kg/m^3)	1900
HDPE geocells	
Strip thickness (mm)	1.5
Young modulus, E (MPa)	235
Poisson's ratio, υ	0.45
Interface shear modulus k_i (MPa/m)	4.4
Interface cohesion, c_i (kPa)	16
Interface friction, φ_i (°)	16.2

excluding the relation of footing size and opening pocket diameter can be studied deeply. The geocell-soil interface cohesion and friction were considered as follows by Oliaei and Kouzegaran (2017):

interface friction angle = atan (0.8 × tan (φ))

interface cohesion = 0.8 × c

where φ and c are the infill soil's friction angle and cohesive strength, respectively. In this study, the interface cohesion and friction always remain at the same values to focus on the effect of infill materials on geocell-reinforced performance and omit the other reinforced parameters. Detailed calculated parameters assigned for soil, geocells, and geocell-soil interfaces are listed in Table 2. Further, Table 3 presents the detailed calculated scheme.

4. Results and discussion

4.1 Pressure – settlement curves

The relationship between loading stress and vertical displacement of all calculated models (eighteen cases) is shown in Fig. 5. 'U_Coh5' in the legend represents the unreinforced case with the Layer 2 cohesion of 5 kPa. 'R_Coh5' represents the geocell-reinforced case, in which the cohesion of infill soil and cover layer (Layer 2) is 5 kPa. In Fig. 5, the cohesive soil subgrade reinforced with geocells of smaller weld distance shows significant bearing capacity improvement. There is a large distance between two curves under the same cohesion of Layer 2 in Fig. 5(a), especially with the increment of footing settlement. However, the corresponding two curves almost overlap for unreinforced and reinforced cases in Fig. 5(b). The bearing capacity of geocell-reinforced subgrade was improved notoriously, no matter what size of geocells, when the higher cohesion soil was selected as infill material. Hence, it can be concluded that the increment of bearing capacity is attributed to the higher cohesion soil rather than geocells. In the past, many researchers emphasized the geocell-reinforced performance (Hegde and Sitharam 2017) from the contribution of geocells' lateral limitation. However, the infill materials instead of geocells can bring more improvement under the condition of higher weld distance. In addition, it can be concluded that the cohesive soil also can be the infill materials, according to Fig. 5. A detailed description of cohesion's effect is shown in the subsequent paragraphs.

Table 3 Details of parametric study

Constant Parameters		Variable Parameter	Calculated Types
			Unreinforced
Layer 1: E_1 = 4.0 MPa c_1 = 20 kPa φ_1 = 20°	Layer 2: E_2 = 4.0 MPa φ_2 = 20°	Layer 2: c_2 = 5 10 15 20 30 40 kPa	356-150 Geocell-reinforced
			660-150 Geocell-reinforced

Note from Fig. 5(a) that some curves almost overlap each other, i.e., 'U_Coh15' and 'R_Coh10', 'U_Coh30' and 'R_Coh15', and 'U_Coh40' and 'R_Coh20'. The equivalent cohesion increases by approximately 5 kPa, 15 kPa, and 20 kPa. However, there are no overlap curves in Fig. 5(b). In sum, the equivalent cohesion of the geocell-reinforced layer is related to weld distance, which is consistent with previous studies (Latha and Somwanshi 2009). Furthermore, The equivalent cohesion increment of the geocell-reinforced layer varied when the IMC differed, despite geocells being the same size.

4.2 Bearing capacity improvement factor (I_f)

Tafreshi and Dawson (2010) used the I_f to evaluate geocell-reinforced improvement of bearing capacity. I_f is a non-dimensional parameter defined as

$$I_f = \frac{q_r}{q_0} \tag{1}$$

Where q_r and q_0 are the bearing capacity of the reinforced and unreinforced subgrade at a given settlement, respectively. In this study, there are many unreinforced cases in which the cohesion of Layer 2 is from 5 kPa to 40 kPa. The bearing capacity of 'U_Coh20' case is considered as the denominator (q_0) here, where the mechanical characteristics between Layer 1 and Layer 2 keep the same in this case.

Variations of I_f for different numerical models are compared in Fig. 6. In some cases, values of I_f <1 are observed, which means the bearing capacity of this case is less than the 'U_Coh20' case. In addition, from Fig. 6, IMC influences the geocell-reinforced performance significantly. All I_f values are also less than 1.0 when IMC is less than 20 kPa, except for the 'R_Coh15' case with weld distance of 356 mm. In addition, I_f values decrease with increasing settlement for the cases with the cohesion of Layer 2 less than 20 kPa. This response is related to the form of pressure–settlement curves. As shown in Fig. 6, the type failure transitions from punching shear to general shear due

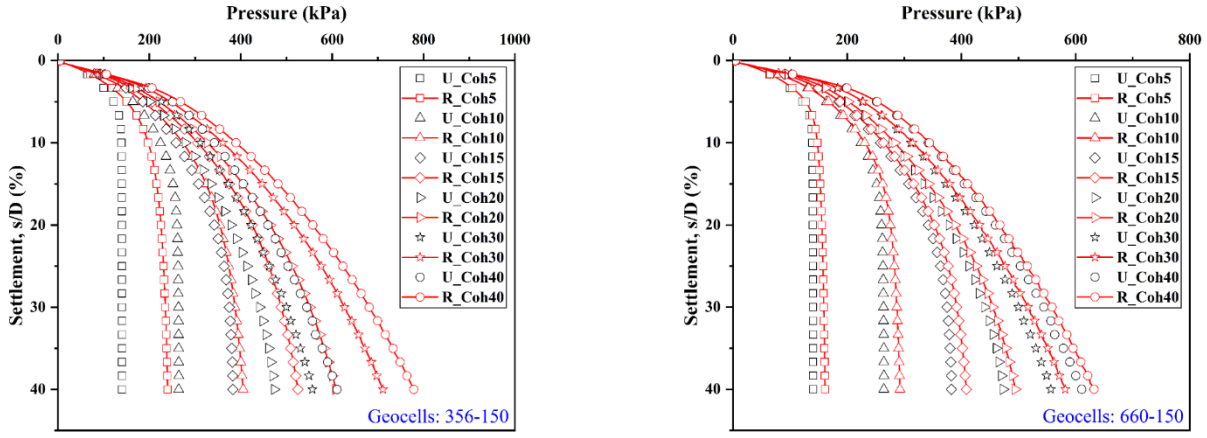

(a) Pressure – settlement curves of unreinforced cases and 356-150 geocell-reinforced cases

(b) Pressure – settlement curves of unreinforced cases and 660-150 geocell-reinforced cases

Fig. 5 Pressure – settlement curves of various numerical models

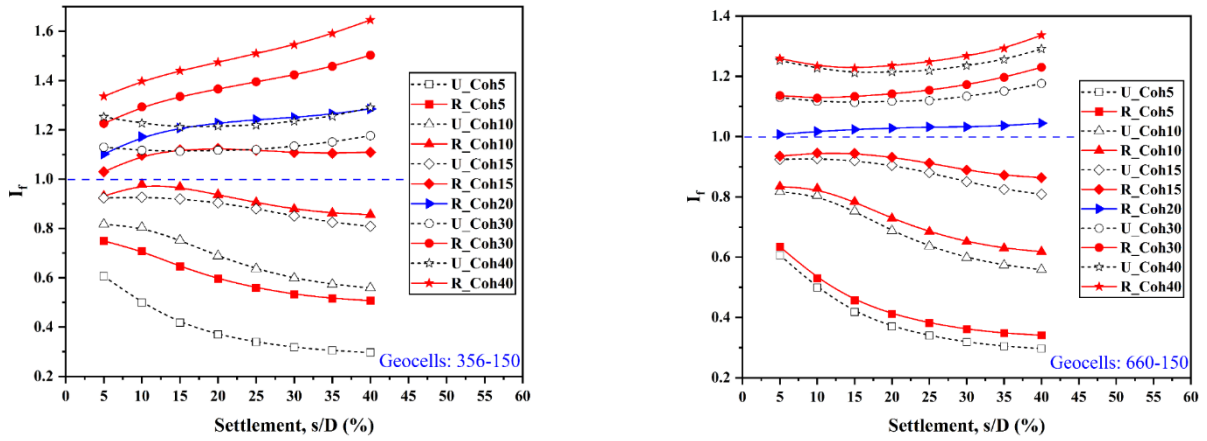

(a) Unreinforced and 356-150 geocell-reinforced cases

(b) Unreinforced and 660-150 geocell-reinforced cases

Fig. 6 Variation of If with footing settlement for different numerical models

to the increase of Layer 2 cohesion. The sharp failure results in the bearing capacity keeping constant, while the bearing capacity of 'U_Coh20' case increases with the settlement. Similar, I_f values increase with the settlement when the Layer 2 cohesion is larger than 20 kPa.

In Fig. 6(a), the curves of 'R_Coh30' and 'R_Coh40' cases present an increasing linear trend, different from the types of 'U_Coh30' and 'U_Coh40' cases (remain almost horizontal). It is worth mentioning that I_f values increase approximately 25.0% and 26.5% with the increase in footing settlement from 5% to 40%, respectively for 'R_Coh30' and 'R_Coh40' cases. Also, subtle differences can also be observed in Fig. 6(b). The footing settlement influences little to the improvement of bearing capacity for 'U_Coh30' and 'U_Coh40' cases. When the soil with cohesion $\geqslant$ 20 kPa was taken as infill materials, the footing settlement significantly affected the geocell-reinforced performance. Geocells are three-dimension honeycomb-shaped geosynthetics fabricated with vertical polymer sheets. The more considerable deformation of infill materials can mobilize the higher lateral limitation. Hence, significant improvement can be observed in Fig. 6 for 'R_Coh20', 'R_Coh30' and 'R_Coh40' cases due to the large footing settlement.

Variations of I_f with different footing settlements are presented in Fig. 7. It can be concluded that infill materials with higher cohesion can improve bearing capacity. However, this result can not suggest that the higher cohesion is beneficial to geocells' contribution. All curves in Fig. 7 show that the growth rate tends to decrease as the IMC increases, indicating that higher cohesion may inhibit the contribution of the geocells. A detailed discussion can be found in the follow-up analysis.

4.3 Contribution of geocells and infill materials

A normalized indicator, the percentage of geocells contribution (PGC_N), was proposed in this study in order to distinguish the respective contributions of geocells and infill materials. Taking the Layer 2 with 10 kPa (cohesion) as an example, it is defined as

$$PGC_N = \frac{q_{R\_Coh10} - q_{U\_Coh10}}{q_{R\_Coh10}} \tag{2}$$

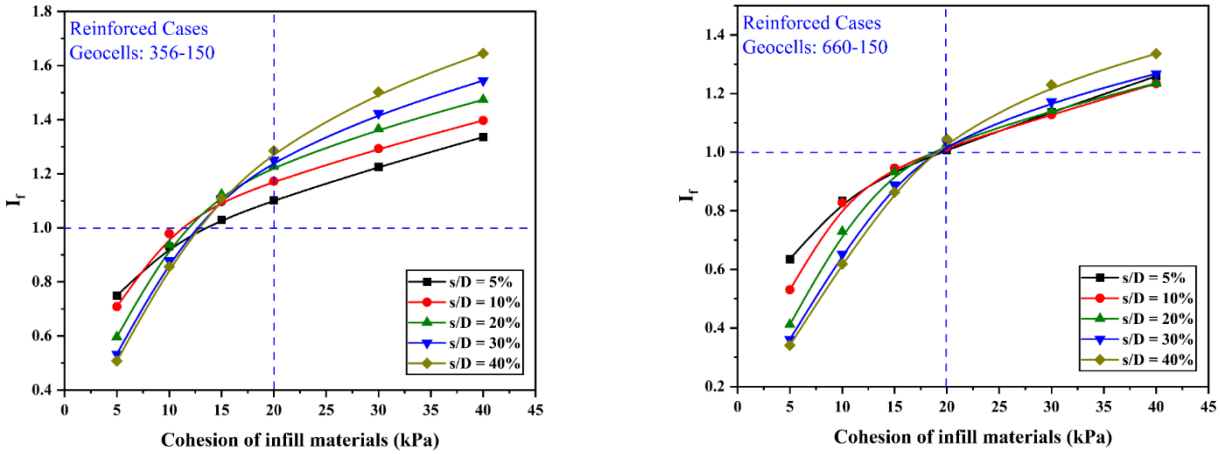

(a) Unreinforced and 356-150 geocell-reinforced cases (b) Unreinforced and 660-150 geocell-reinforced cases

Fig. 7 Variation of If with infill materials' cohesin for different footing settlement

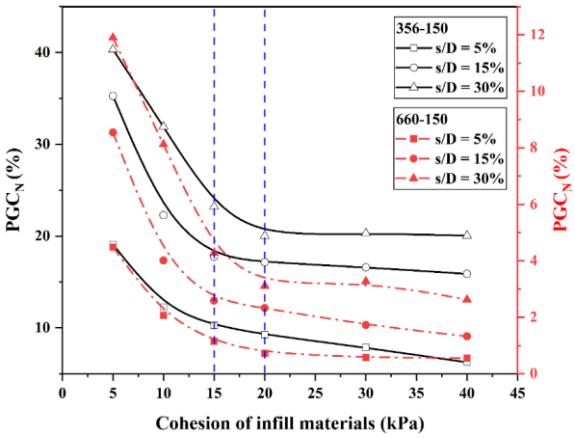

Fig. 8 Variation of PGC_N with IMC for different footing settlement

Where q_{R_Coh10} d q_{U_Coh10} e the bearing capacity of 'R_Coh10' and 'U_Coh10' cases at a given footing settlement, respectively. The results from numerical models are included in Fig. 8. The PGC_N values of geocells with weld distance of 356 mm vary between 5% and 40%, while values of geocells with weld distance of 660 mm vary between 0.5% and 12%. This response reveals that geocells with small weld distance (356 mm) contribute more to bearing capacity compared to geocells with the large weld distance (660 mm). Various researchers also made similar observations (Gedela *et al.* 2021). Also, in Fig. 8, PGC_N values increase with the increment of footing settlement. The effect of lateral limitation is exploited due to the larger lateral deformation caused by vertical footing settlement, which benefits geocells' contribution.

Furthermore, it can be seen that all curves presented in Fig. 8 decrease sharply and flattens out gradually. The demarcation line lies between approximately 15 kPa and 20 kPa on X-axis. Geocells' contribution decreases linearly with increasing cohesion when IMC is less than the threshold value. On the other hand, geocells' contribution remains almost constant for IMC exceeds the threshold value. Taking the 356-150 geocells at the case of *s/D* = 15% as an example, it is observed that a 50.6% drop in PGC_N values with the increase in IMC from 5 kPa to 15 kPa. On the other hand, with the increase in IMC from 15 kPa to 40 kPa, approximately 10.2% times reduction in PGC_N values is observed. The results suggest that the selected IMC should be less than 15 kPa or 20 kPa to acquire the higher geocells' contribution (lateral limitation effect) in bearing capacity.

5. Mechanism

The influence of IMC on bearing capacity was studied in Section Four. All results were obtained from pressure–settlement responses. Also, some interesting conclusions were proposed based on these. However, the mechanism of these conclusions is still not yet precise. In the following, the deformation of subgrade, vertical coupling shear stress, confining stress and deformation of geocells are analyzed to discuss the mechanism on the influence of IMC on reinforced performance.

5.1 Vectors and contours of soils' deformations

Taking the numerical models of 356-150 geocell-reinforced subgrade as examples, the total displacement vectors (unit as m) at s/D = 40% with different IMC on the plane of Y = 0 are present in Fig. 9. Geocell models are omitted in the figures to show more clearly. From Figs. 9(a) -9(c), soil heave around the applied area is detected. On the other hand, this heave is restrained by the increasing IMC, shown in Figs. 9(d) - 9(f). Dash *et al.* (2001) claimed that geocells could limit soil heaving. However, the infill materials also influence it. In addition, it can be seen that the blue vectors, represented as the maximum vertical displacement, gradually move deeper and deeper. In order to quantify the detailed vertical deformation, Z-direction deformation contours (unit as mm) of models on the plane of X = 0 are present in Fig. 10. Similar to Fig. 9, the blue color area, which presents the vertical displacement range from 110 mm to 120 mm, increases gradually and

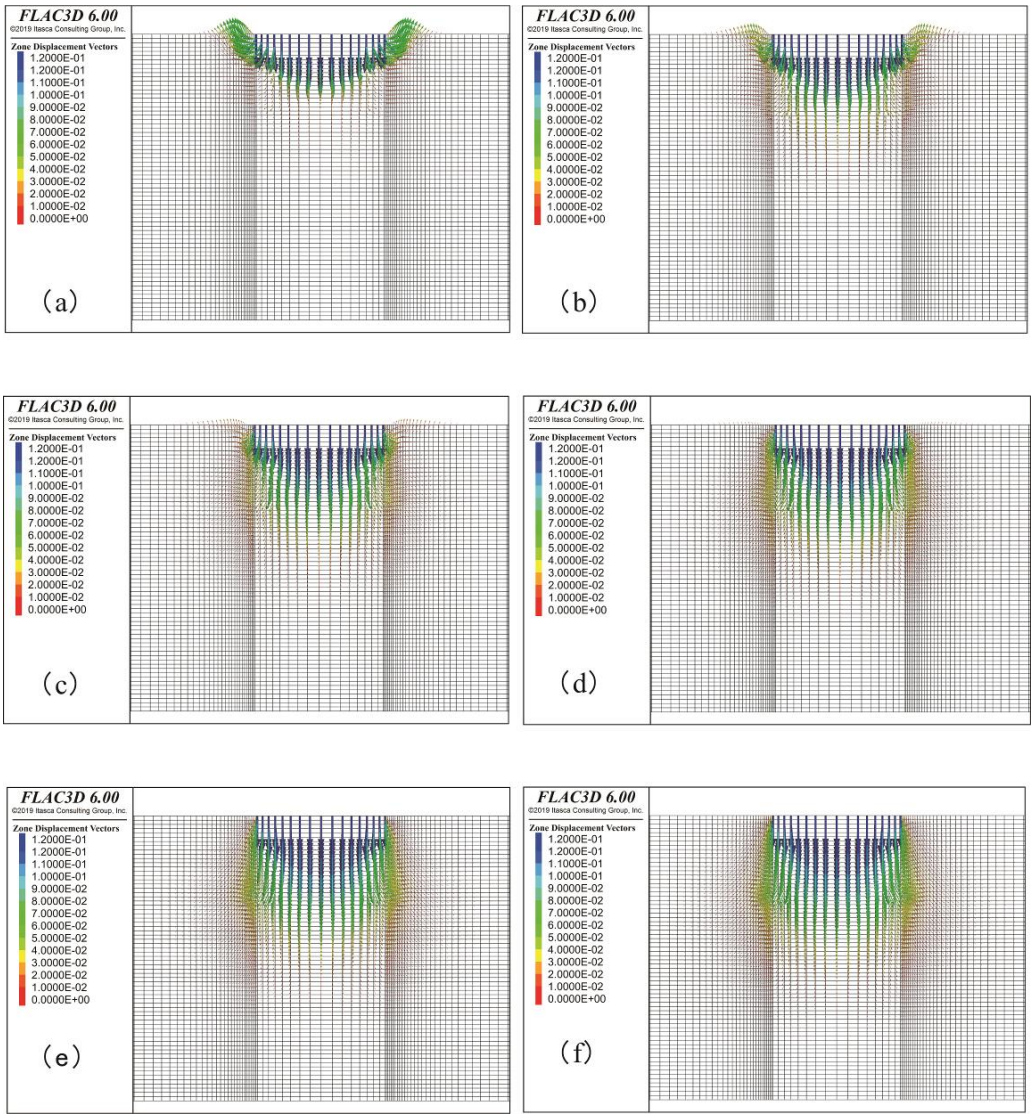

Fig. 9 Total displacement vectors for models with IMC of (a) 5 kPa, (b) 10 kPa, (c) 15 kPa, (d) 20 kPa, (e) 30 kPa and (f) 40 kPa

progresses deeper. The central displacement at the bottom of the geocell-reinforced layer was extracted to illustrate this response clearly. As shown in Fig. 11, with the increase of IMC, this absolute value of vertical deformation increases sharply and gradually tend to be stable. The central vertical displacement is -22 mm, -79 mm and -92 mm, respectively, at the IMC of 5 kPa, 20 kPa and 40 kPa. It is observed that 2.6 times increment with the increase in IMC from 5 kPa to 20 kPa. Nevertheless, only 0.16 times increment is observed with the increase in IMC from 20 kPa to 40 kPa.

Combined with the results shown in Section 4, it can be concluded that the displacement trend in the subgrade is related to geocells' contribution and bearing capacity. A preliminary conclusion can be made that the total displacement under loading area towards to vertical rather than lateral direction with the increase of IMC. Also, this deformation trend influences the entire bearing capacity and geocells' contribution. 1) Vertical displacements toward deeper depth can allow more soil to resist the applied load, benefiting the bearing capacity. Hence, the reinforced cases of infill materials with higher cohesion present greater bearing capacity. 2) The greater bearing capacity is attributed to higher IMC than the lateral limitation of geocells. The total deformation develops to the vertical deeper area, not lateral direction, which is not conducive to geocells' lateral limitation effect and decreases geocells' contribution to bearing capacity. The deformation along the X or Y direction of the subgrade is related closely to the lateral deformation of geocell walls. The following description will analyze it deeply.

5.2 Coupling shear stress and confining stress of geocell walls

The main reinforcing factors are vertical resistance, lateral limitation, and membrane effect. The membrane effect only works in the case that the geocell-reinforced layer is significantly deformed and the geocell mattress is very wide. Hence, in this study, only the vertical coupling

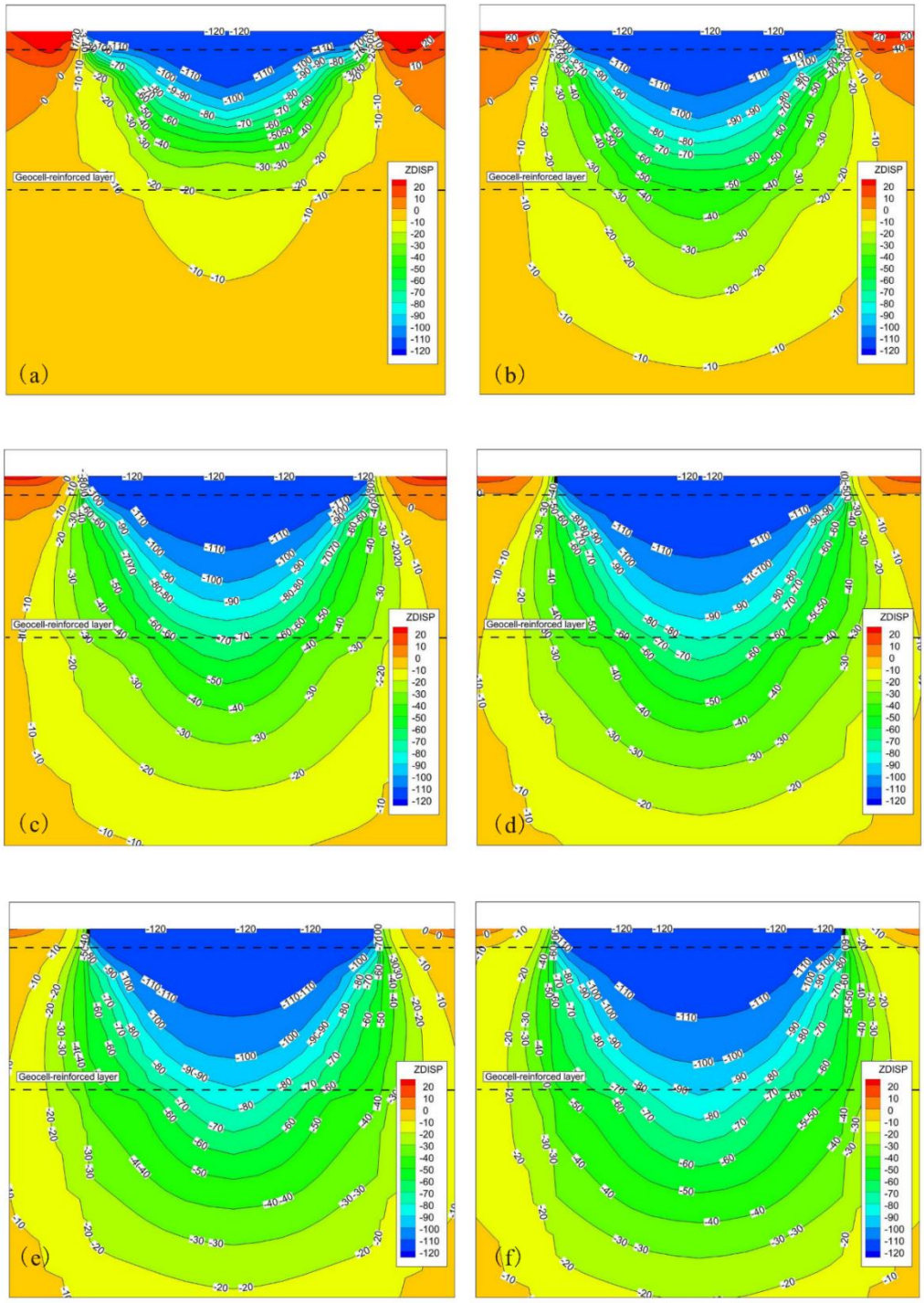

Fig. 10 Vertical displacement contours for models with IMC of (a) 5 kPa, (b) 10 kPa, (c) 15 kPa, (d) 20 kPa, (e) 30 kPa and (f) 40 kPa

shear stress and confining stress of geocell walls were analyzed to understand the influence of IMC on bearing capacity. It is worth noting that the values presented in this section are the average values of four geocell walls nearest the loading area. A series of FISH codes were programmed to add up the monitoring data from all elements or nodes in numerical calculations. Then, the average values were obtained by dividing the sum by the number of nodes or elements.

Figs. 12 and 13 illustrate the relationship of coupling shear stress and confining stress, respectively with applied load for cases with various IMC. The stress values of geocell-reinforced cases with larger weld distances are smaller due to geocell walls far from the loading area. Initially, the coupling shear stress and confining stress increase slowly with the increase of applied pressure. However, there is a sharp increment once the applied load exceeds a given pressure. Combined with the settlement–

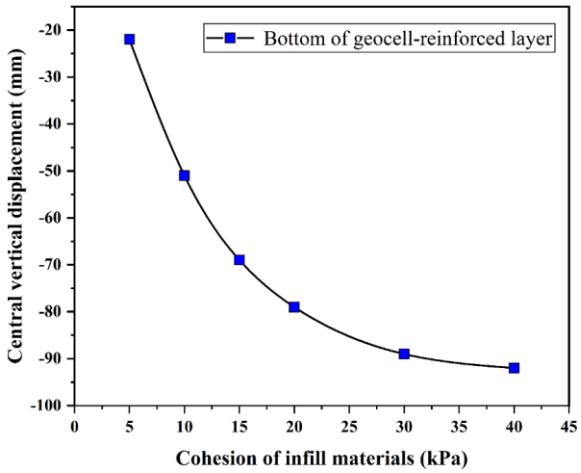

Fig. 11 Variation of central vertical displacement at the bottom of reinforced layer for numerical models with various IMC

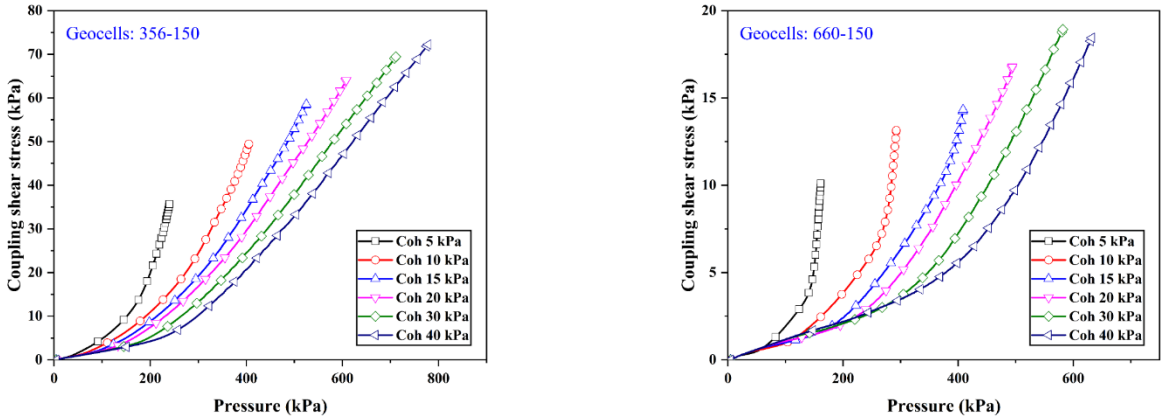

(a) 356-150 geocells reinforcement (b) 660-150 geocells reinforcement

Fig. 12 Variation of coupling shear stress for the cases with various IMC

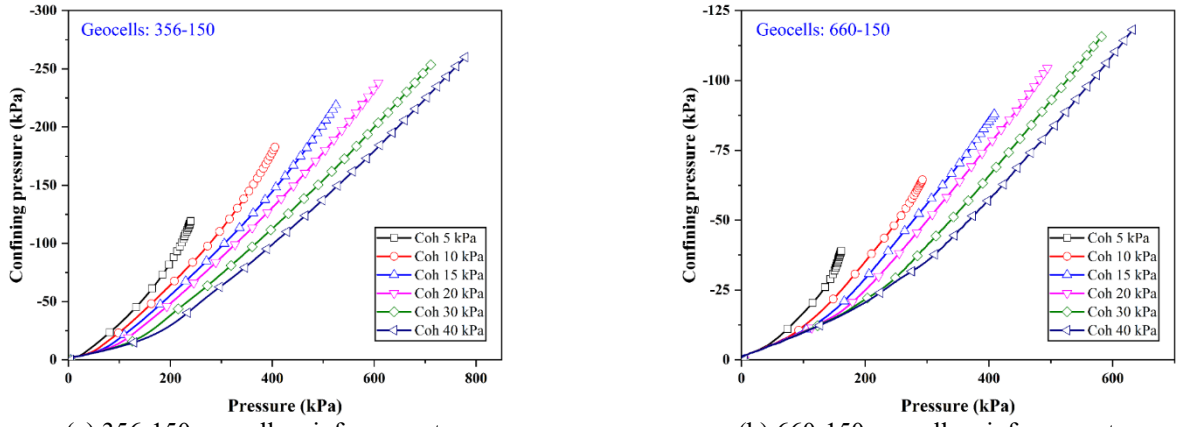

(a) 356-150 geocells reinforcement (b) 660-150 geocells reinforcement

Fig. 13 Variation of confining stress for the cases with various IMC

pressure responses curves in Fig. 5, this threshold value corresponds to allowable bearing capacity. A subtle increment of applied pressure results in a large deformation when the applied pressure is larger than the threshold value. It makes the coupling shear stress and confining stress increase sharply.

In addition, the higher IMC, the smaller shear and confining stress under the same applied load. Fig. 5 shows that the footing displacement is more minor, when the cohesion of adopted infill materials is higher under the same pressure. Also, Fig. 9 to Fig. 11 show that the infill soils with higher cohesion make the entire deformation mainly toward to vertical, not lateral direction. The

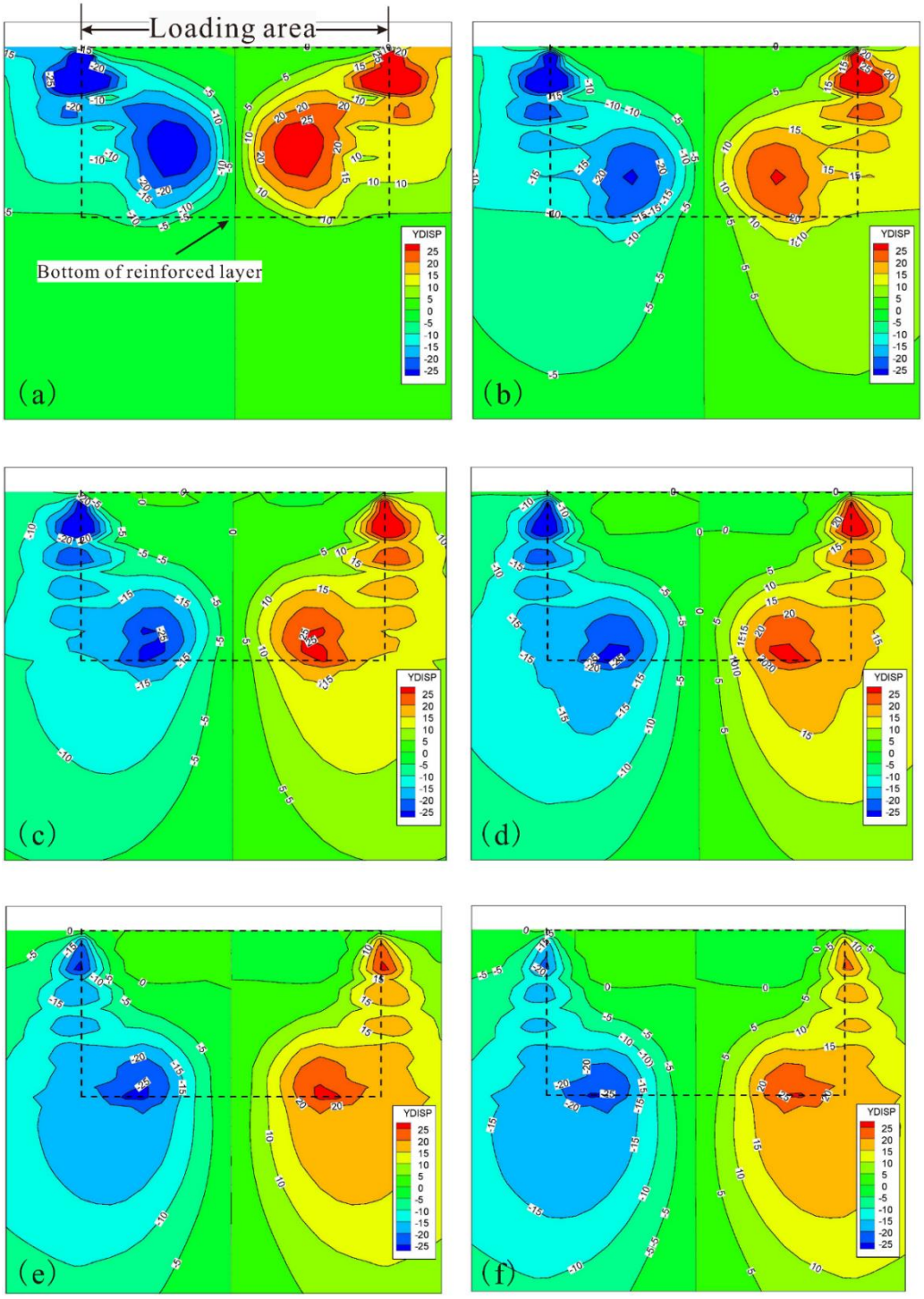

Fig. 14 Lateral displacement contours for models with IMC of (a) 5 kPa, (b) 10 kPa, (c) 15 kPa, (d) 20 kPa, (e) 30 kPa and (f) 40 kPa

coupling of these two factors weakens the lateral limitation effect, contributing to the decreasing of coupling shear stress and confining stress under the same applied pressure.

5.3 Lateral deformation of subgrade and geocell walls

In Section 5.1, the results indicated that the subgrade deformation mainly toward vertical rather than lateral direction. Hence, the lateral deformations of subgrade and geocell walls are presented to verify this preliminary conclusion. Taking the numerical models of 356-150 geocell-reinforced subgrade as examples, Fig. 14 shows the lateral deformation (in Y direction) contours, unit as mm, of models at s/D = 40% on the plane of X = 0 for the cases with various IMC. The darkest colored red and blue areas represent the lateral displacements greater than 25 mm, and

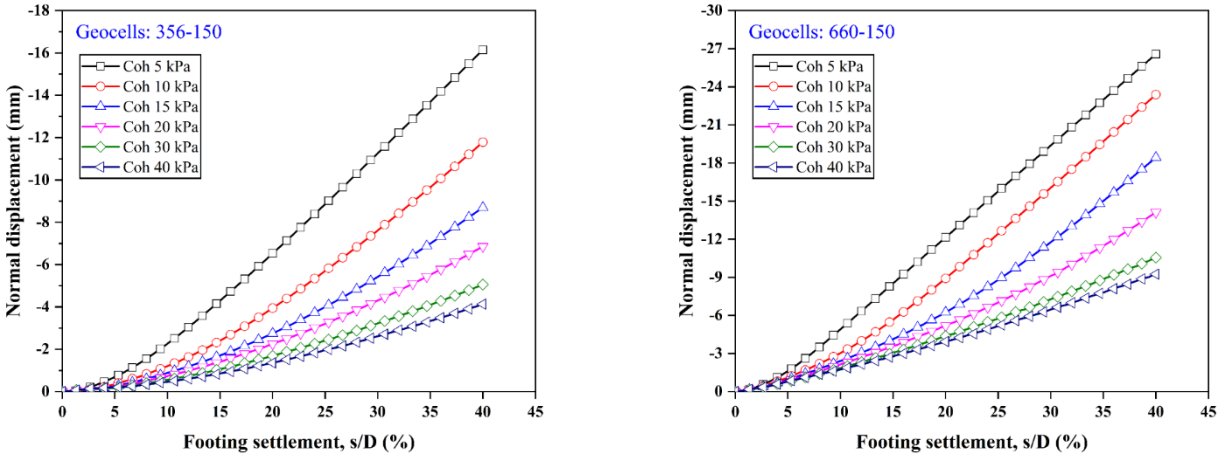

(a) 356-150 geocells reinforcement (b) 660-150 geocells reinforcement

Fig. 15 Variation of normal displacement for the cases with various IMC

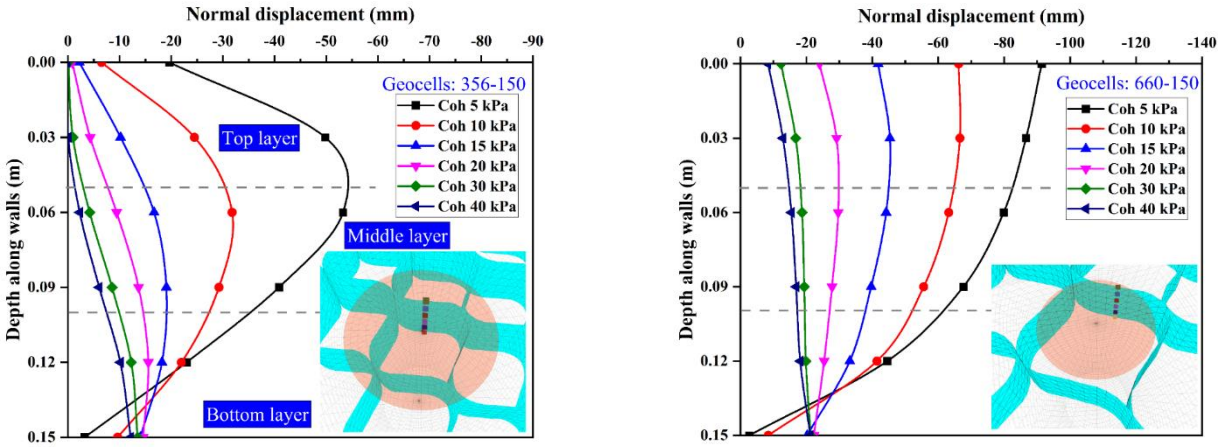

(a) 356-150 geocells (b) 660-150 geocells

Fig. 16 Normal displacement along walls for numerical models with various IMC

they are located in the upper right or upper left corner of the figure, decreasing as the IMC increases. Moreover, the darkest colored red and blue areas located in the central region also reduce and move in the lateral direction. It indicates that the lateral displacement at the geocell-reinforced layer decreases. Also, deeper soil layers are mobilized, resulting in lateral displacements in the soil layer below the geocell-reinforced layer.

In FLAC^{3D}, the geogrid elements and soils can be misaligned along the tangential direction, but are always fixed together along the normal direction. Hence, the lateral deformations of geocell walls are inevitably related to the results presented in Fig. 14. Also, the normal displacement of geocell walls is the definitive parameter judging the geocells' lateral limitation effect and geocells' contribution. Same as Section 5.2, the normal displacement is the average normal displacement of four geocell walls nearest the loading area. Fig. 15 presents the variation of geocell normal displacement with footing settlement for the cases with various IMC. The normal displacement of geocell with weld distance of 660 mm is larger than the values of geocell with weld distance of 356 mm, because of geocell walls outside loading area. Nevertheless, more walls are mobilized for geocells with small weld distances under the applied pressure, where the vertical frictional resistance mainly improves the bearing capacity. In addition, regardless of geocell pocket size, the higher IMC results in the small normal displacement of geocell walls under the same footing settlement, which weakens the lateral limitation effect of geocells.

Fig. 16 shows the normal displacement of recorded points of geocell walls along the vertical direction with various infill materials under s/D = 40%. This figure makes it easier to recognize the evolution of geocells' deformation. No matter what the size of geocells, the normal displacement of geocell walls in the case that IMC is 5 kPa is larger. The normal displacement gradually decreases with the increase of IMC. In Fig. 16(a), the point of largest normal displacement transfers from the dividing line between the top and middle layers to the bottom of the walls. In Fig. 16(b), the point of largest normal displacement is located at the top of walls for the case of infill materials' of 5 kPa. The relationship between loading area and opening pock size results in this difference. The

results of lateral (normal) displacement of geocell walls again prove that the higher IMC contributes to the soils' deformation mainly toward to vertical rather than lateral direction. This response makes the effect of lateral limitation more significant and weak the contribution of geocells in bearing capacity.

6. Conclusions

In this present study, the soil of low cohesion is recommended to fill geocell pockets to increase the contributions of geocell. Also, adopting infill materials with high cohesion can improve bearing capacity significantly. It seems that the two conclusions run counter to each other. However, different viewpoints lead to this contradiction. From the view of the lateral limitation of geocell, infill materials with low cohesion are recommended. From the view of improving the bearing capacity, the infill materials with high cohesion are the optimal filler. It is crucial to note that the internal friction of infill materials is constant for all numerical models in this study. In site engineering, the cohesionless soil usually exhibits larger internal friction. Hence, adopting sandy soil as infill materials also can improve the bearing capacity. This paper omits the changing of internal friction to focus on the influence of cohesion on geocell-reinforced performance and aims to deeply discuss the reasons and mechanisms. Moreover, the higher internal friction (or dilation) may weaken or enhance the geocells' contribution. This extrapolation also needs to be validated. The following studies should conduct model tests, adopting the sand, silt, and clay soil as infill materials, to analyze the total deformation vectors based on the Digital Imaging Correlation Techniques.

This study focused on the effect of IMC on geocell-reinforced performance. From the view of pressure-settlement responses, the bearing capacity improvement was compared by using the soils with various cohesion as infill materials. Contributions of geocells were evaluated by I_f and PGC_N. Further, the mechanism of cohesive soil inhibiting the effect of geocell lateral limitation was deeply studied by the vertical and lateral deformation of subgrade, coupling shear stress and confining stress of geocells, and deformation of geocells. Based on these observations, the following conclusion can be drawn:

(1) According to pressure and settlement response, using the soil with high cohesion as infill materials can significantly improve the bearing capacity. The type failure transitions from punching shear to general shear with the increment of IMC. In addition, geocells can improve the equivalent cohesion of the reinforced layer from the overlapped pressure-settlement curves. However, various IMC improves equivalent cohesion of geocell-reinforced layer, even the used geocells keep identical size, which is different from the results obtained from triaxial tests.

(2) I_f and PGC_N were adopted to assess the contributions of geocells on bearing capacity in this study. Although adopting the infill materials with higher cohesion can contribute to bearing capacity, geocells' contribution is decreased sharply with the increase of IMC as anticipated. In addition, it can be concluded that geocells with a small weld distance contribute more to bearing capacity, as compared to geocells with a large weld distance.

(3) The vertical and lateral deformation contours of subgrade all revealed the total displacement towards deeper depth. This response results in the lateral deformation of the geocell-reinforced layer decreasing and higher lateral displacements occurring in the soil layer below the geocell-reinforced layer. A larger soil region is mobilized to benefit bearing capacity, but the lateral limitation effect of geocells is diminished.

(4) The higher IMC, the smaller shear and confining stress under the same applied load. Further, the average normal displacement of geocell walls decreases with the increase of IMC. Regardless of any geocell size, the point of largest normal displacement moves from the top layer to the bottom layer. These results also validate the law of subgrade total deformation.

(5) The authors hold the opinion that the present study progresses to understand the influence of IMC on bearing capacity. It interprets the reasons and mechanism that cohesion inhibits the lateral limitation of geocells, which can guide the researchers and designers in selecting the optimum infill soils.

Acknowledgments

The research described in this paper was financially supported by the National Natural Science Foundation of China (Nos. 42077262, 42077261, and 41972294)

References

Altay, G., Kayadelen, C., Canakci, H., Bagriacik, B., Ok, B. and Oguzhanoglu, M.A. (2021), "Experimental investigation of deformation behavior of geocell retaining walls", *Geomech. Eng.*, **27**(5), 419-431. https://doi.org/10.12989/gae.2021.27.5.419.

Ardakani, A. and Namaei, A. (2021), "Numerical investigation of geocell reinforced slopes behavior by considering geocell geometry effect", *Geomech. Eng.*, **24**(6), 589-597. https://doi.org/10.12989/gae.2021.24.6.589.

Ari, A. and Misir, G. (2021), "Three-dimensional numerical analysis of geocell reinforced shell foundations", *Geotext. Geomembranes*, **49**(4), 963-975. https://doi.org/10.1016/j.geotexmem.2021.01.006.

Bathurst, R.J. and Karpurapu, R. (1993), "Large-scale triaxial compression testing of geocell-reinforced granular soils", *Geotech. Test. J.*, **16**(3), 296-303. https://doi.org/10.1016/0148-9062(94)93106-2.

Biswas, A., Murali Krishna, A. and Dash, S. K. (2013), "Influence of subgrade strength on the performance of geocell-reinforced foundation systems", *Geosynth. Int.*, **20**(6), 376-388. https://doi.org/10.1680/gein.13.00025.

Biswas, S., Hussain, M. and Singh, K.L. (2021), "Behaviour of jute and bamboo geocell with additional basal mat filled with different infill materials overlaying soft subgrade", *Int. J. Geosynth. Ground Eng.*, **7**(3), https://doi.org/10.1007/s40891-021-00297-4

Biswas, S. and Mittal, S. (2017), "Square footing on geocell reinforced cohesionless soils", *Geomech. Eng.*, **13**(4), 641-651.

https://doi.org/10.12989/gae.2017.13.4.641.

Chaney, R.C., Demars, K.R., Krishnaswamy, N.R., Rajagopal, K. and Madhavi Latha, G. (2000), "Model studies on geocell supported embankments constructed over a soft clay foundation", *Geotech. Test. J.*, **23**(1), 45-54. https://doi.org/10.1520/gtj11122j

Dash, S.K., Krishnaswamy, N.R. and Rajagopal, K. (2001), "Bearing capacity of strip footings supported on geocell-reinforced sand", *Geotext. Geomembranes*, **19**(4), 235-256. https://doi.org/10.1016/S0266-1144(01)00006-1

Dehkordi, P.F., Ghazavi, M., Ganjian, N. and Karim, U.F.A. (2019), "Effect of geocell-reinforced sand base on bearing capacity of twin circular footings", *Geosynth. Int.*, **26**(3), 224-236. https://doi.org/10.1680/jgein.19.00047.

Dutta, S. and Mandal, J.N. (2016), "Model studies on geocell-reinforced fly ash bed overlying soft clay", *J. Mater. Civil Eng.*, **28**(2), 04015091. https://doi.org/10.1061/(ASCE)MT.1943-5533.0001356.

Gedela, R., Kalla, S., Sudarsanan, N. and Karpurapu, R. (2021), "Assessment of Load Distribution Mechanism in Geocell Reinforced Foundation Beds using Digital Imaging Correlation Techniques. *Transp. Geotech.*, No. 100664. https://doi.org/10.1016/j.trgeo.2021.100664.

Gedela, R. and Karpurapu, R. (2021a), "Influence of pocket shape on numerical response of geocell reinforced foundation systems", *Geosynth. Int.*, **28**(3), 327-337. https://doi.org/10.1680/jgein.20.00042.

Gedela, R. and Karpurapu, R. (2021b), "Laboratory and numerical studies on the performance of geocell reinforced base layer overlying soft subgrade", *Int. J. Geosynth. Ground Eng.*, **7**(1), 1-18. https://doi.org/10.1007/s40891-020-00249-4.

George, A.M., Banerjee, A., Puppala, A.J. and Saladhi, M. (2021), "Performance evaluation of geocell-reinforced reclaimed asphalt pavement (RAP) bases in flexible pavements", *Int. J. Pavement Eng.*, **22**(2), 181-191. https://doi.org/10.1080/10298436.2019.1587437.

Hegde, A. and Sitharam, T.G. (2016), "Behaviour of geocell reinforced soft clay bed subjected to incremental cyclic loading", *Geomech. Eng.*, **10**(4), 405-422. https://doi.org/10.12989/gae.2016.10.4.405.

Hegde, A. and Sitharam, T.G. (2017), "Experiment and 3D-numerical studies on soft clay bed reinforced with different types of cellular confinement systems", *Transp. Geotech.*, **10**, 73-84. https://doi.org/10.1016/j.trgeo.2017.01.001.

Hegde, A.M. and Sitharam, T.G. (2015), "Effect of infill materials on the performance of geocell reinforced soft clay beds", *Geomech. Geoeng.*, **10**(3), 163-173. https://doi.org/10.1080/17486025.2014.921334.

Itasca (2018), Fast Lagrangian Analysis of Continua (FLAC3D 6.0). Itasca Consulting Group Inc, Minneapolis, USA.

Kargar, M. and Mir Mohammad Hosseini, S.M. (2018), "Influence of reinforcement stiffness and strength on load-settlement response of geocell-reinforced sand bases", *Eur. J. Environ. Civil Eng.*, **22**(5), 596-613. https://doi.org/10.1080/19648189.2016.1214181.

Khalaj, O., Tafreshi, S.N.M., Masek, B. and Dawson, A.R. (2015), "Improvement of pavement foundation response with multi-layers of geocell reinforcement: Cyclic plate load test", *Geomech. Eng.*, **9**(3), 373-395. https://doi.org/10.12989/gae.2015.9.3.373.

Kumar, A., Singh, A.P. and Chatterjee, K. (2019), "Ground improvement using geocells to enhance trafficability in desert soils", *Geomech. Eng.*, **19**(1), 71-78. https://doi.org/10.12989/gae.2019.19.1.071.

Latha, G.M. (2011), "Design of geocell reinforcement for supporting embankments on soft ground", *Geomech. Eng.*, **3**(2), 117-130. https://doi.org/10.12989/gae.2011.3.2.117.

Latha, G.M. and Somwanshi, A. (2009), "Effect of reinforcement form on the bearing capacity of square footings on sand", *Geotext. Geomembranes*, **27**(6), 409-422. https://doi.org/10.1016/j.geotexmem.2009.03.005.

Lu, Z., Xian, S., Yao, H., Fang, R. and She, J. (2019), "Influence of freeze-thaw cycles in the presence of a supplementary water supply on mechanical properties of compacted soil", *Cold Reg. Sci. Technol.*, **157**, 42-52. https://doi.org/10.1016/j.coldregions.2018.09.009.

Luo, X., Lu, Z., Yao, H., Zhang, J. and Song, W. (2021), "Experimental study on soft rock subgrade reinforced with geocell", *Road Mater. Pavement Design*, 1-15. https://doi.org/10.1080/14680629.2021.1948907.

Moghaddas Tafreshi, S.N., Rafiezadeh Malekshah, A., Rahimi, M. and Dawson, A.R. (2021), "Bearing capacity improvement using soil-filled post-consumer PET bottles", *Geosynth. Int.*, 1-29. https://doi.org/10.1680/jgein.21.00031.

Moghaddas Tafreshi, S.N., Sharifi, P. and Dawson, A.R. (2016), "Performance of circular footings on sand by use of multiple-geocell or -planar geotextile reinforcing layers", *Soils Found.*, **56**(6), 984-997. https://doi.org/10.1016/j.sandf.2016.11.004.

Oliaei, M. and Kouzegaran, S. (2017), "Efficiency of cellular geosynthetics for foundation reinforcement", *Geotext. Geomembranes*, **45**(2), 11-22. https://doi.org/10.1016/j.geotexmem.2016.11.001.

Pokharel, S.K., Han, J., Leshchinsky, D., Parsons, R.L. and Halahmi, I. (2010), "Investigation of factors influencing behavior of single geocell-reinforced bases under static loading", *Geotext. Geomembranes*, **28**(6), 570-578. https://doi.org/10.1016/j.geotexmem.2010.06.002.

Saride, S., Pradhan, S., Sitharam, T.G. and Puppala, A.J. (2013), "Numerical analysis of geocell reinforced ballast overlying soft clay subgrade", *Geomech. Eng.*, **5**(3), 263-281. https://doi.org/10.12989/gae.2013.5.3.263.

Sheikh, I.R. and Shah, M.Y. (2020), "State-of-the-art review on the role of geocells in soil reinforcement", *Geotech. Geol. Eng.*, **39**(3), 1727-1741. https://doi.org/10.1007/s10706-020-01629-3.

Sireesh, S., Sitharam, T.G. and Dash, S.K. (2009), "Bearing capacity of circular footing on geocell–sand mattress overlying clay bed with void", *Geotext. Geomembranes*, **27**(2), 89-98. https://doi.org/10.1016/j.geotexmem.2008.09.005.

Sitharam, T.G. and Hegde, A. (2013), "Design and construction of geocell foundation to support the embankment on settled red mud", *Geotext. Geomembranes*, **41**, 55-63. https://doi.org/10.1016/j.geotexmem.2013.08.005.

Sitharam, T.G. and Sireesh, S. (2005), "Behavior of embedded footings supported on geogrid cell reinforced foundation beds", *Geotech. Test. J.*, **28**(5), 452-463. https://doi.org/10.1520/GTJ12751.

Song, F. and Tian, Y. (2019), "Three-dimensional numerical modelling of geocell reinforced soils and its practical application", *Geomech. Eng.*, **17**(1), 1-9. https://doi.org/10.12989/gae.2019.17.1.001.

Suku, L., Prabhu, S.S., Ramesh, P. and Babu, G.L.S. (2016), "Behavior of geocell-reinforced granular base under repeated loading", *Transp. Geotech.*, **9**, 17-30. https://doi.org/10.1016/j.trgeo.2016.06.002.

Tafreshi, S.N.M., Darabi, N.J. and Dawson, A.R. (2018), "Cyclic loading response of footing on multilayered rubber-soil mixtures", *Geomech. Eng.*, **14**(2), 115-129. https://doi.org/10.12989/gae.2018.14.2.115.

Tafreshi, S.N.M. and Dawson, A.R. (2010), "Comparison of bearing capacity of a strip footing on sand with geocell and with planar forms of geotextile reinforcement", *Geotext. Geomembranes*, **28**(1), 72-84. https://doi.org/10.1016/j.geotexmem.2009.09.003.

Thakur, J.K., Han, J. and Parsons, R.L. (2017), "Factors

influencing deformations of geocell-reinforced recycled asphalt pavement bases under cyclic loading", *J. Mater. Civil Eng.*, **29**(3), 04016240. https://doi.org/10.1061/(asce)mt.1943-5533.0001760.

Thakur, J.K., Han, J., Pokharel, S.K. and Parsons, R.L. (2012), "Performance of geocell-reinforced recycled asphalt pavement (RAP) bases over weak subgrade under cyclic plate loading", *Geotext. Geomembranes*, **35**, 14-24. https://doi.org/10.1016/j.geotexmem.2012.06.004.

Thallak, S.G., Saride, S. and Dash, S.K. (2007), "Performance of surface footing on geocell-reinforced soft clay beds", *Geotech. Geol. Eng.*, **25**(5), 509-524. https://doi.org/10.1007/s10706-007-9125-8.

Xian, S. (2019), "Study on mechanical properties and service performance of levee filling in deep seasonal frozen regions", Ph.D., Institute of Rock and Soil Mechanics, Chinese Academy of Sciences.

JS